LAWRENCE
LIVERMORE
NATIONAL
LABORATORY

UCRL-JRNL-203141

Polishing Slurry Induced Surface Haze on Phosphate Laser Glasses

T. I. Suratwala, P. E. Miller, P. R. Ehrmann,and R. A. Steele

March 1, 2004

Journal of Non-Crystalline Solids

Disclaimer

Polishing slurry induced surface haze on phosphate laser glasses

T. I. Suratwala*, P. E. Miller, P. R. Ehrmann, R. A. Steele
Lawrence Livermore National Laboratory, P.O. Box 808, Livermore, CA 94551, USA

Keywords: metaphosphate glass, cerium oxide, contrast, surface pits, scatter, roughness, AFM, high-peak-power lasers, National Ignition Facility

The effects of residual polishing slurry on the surface topology of highly-polished, Nd-doped metaphosphate laser glasses are reported. Glass samples were pitched polished using cerium oxide or zirconium oxide slurry at different pHs and then washed by different methods that allowed varying amounts of residual slurry to 'dry' on the surface. Upon re-washing with water, some of the samples showed surface haze (scatter), which scaled with the amount of residual slurry. Profilometry measurements showed that the haze is the result of shallow surface pits (100 nm - 20 μm wide x ~15 nm deep). Chemical analyses of material removed during rewashing, confirmed the removal of glass components as well as the preferential removal of modifier ions (e.g. K^{1+} and Mg^{2+}). The surface pits appear to result from reaction of the glass with condensed liquid at the slurry particle-glass interface that produces water-soluble phosphate products that dissolves away with subsequent water contact. Aggressive washing, to remove residual slurry immediately following polishing, can minimize surface haze on phosphate glasses. It is desirable to eliminate haze from glass used in high-peak-power lasers, since it can cause scatter-induced optical modulation that can cause damage to downstream optics.

PACS 81.05.Kf; 81.65.Ps; 81.65.Cf; 82.65.Yh; 42.70Hj

1. Introduction

* Corresponding author. Tel.: +1-925 422 1884; fax +1-925 423 0792. E-mail address: suratwala1@llnl.gov (T.I. Suratwala)

Over 7500 0.4-1 m size optics are currently being manufactured for the National Ignition Facility (NIF), which is a high-peak-power laser for use in fusion energy research [1-3]. Large optics for high power lasers, such as NIF, require high quality optical surfaces (typically λ/3 surface finish and 2-10 Å rms surface roughness) in order to maintain a uniform wavefront and to minimize surface scatter of the passing laser light [2,4]. Increased scatter due to increased roughness degrades the beam quality by producing unacceptable intensity modulation (noise) that increase the probability for damage to downstream optics and components.

The majority of NIF optics, which are fabricated from primarily fused silica, borosilicate, or phosphate [5-6] based glasses, are finished by pitch polishing using an aqueous CeO_{2-x} slurry. It is well known that polishing slurry, if left to dry on freshly polished surfaces, can stain optical glasses. For example in his classic book *"Fabrication Methods for Precision Optics",* Karow [4] states, "the very large number of these tiny particles is the source of haze, stains, and spots on the surface". Despite such longstanding empirical knowledge, the specific nature of the surface degradation is not well understood.

From the considerable work that has been done on the scientific study of glass polishing, it is known that the polishing of oxide glasses occurs by a chemical-mechanical polishing (CMP) mechanism. Specifically, the polishing process involves both chemical interactions, such as hydration, as well as purely mechanical interactions, such as indention fracture [7-12]. In the present study we examine the surface degradation resulting from the interaction of aqueous polishing slurry and highly-polished Nd-doped meta-phosphate glass following the polishing process. Meta-phosphate glass was chosen for the present study both because of its widespread use as the gain media in high power lasers and because it is the least durable of the three primary optical glasses used in NIF.

2. Experimental

2.1 Sample preparation

Two commercial Nd-doped meta-phosphate glasses (LG-770 from Schott Glass Technologies and LHG-8 from Hoya Corporation, USA) were used in the present study. The approximate composition of LG-770 is (58-62wt%) P_2O_5 - (6-10wt%) Al_2O_3 - (20-25wt%) K_2O - (5-10wt%) MgO - (0-2wt%) Nd_2O_3 and of LHG-8 is (56-60wt%) P_2O_5 - (8-12wt%) Al_2O_3 - (13-17wt%) K_2O - (10-15wt%) BaO - (0-2wt%) Nd_2O_3 [5,6]. The major difference in these glasses is the group II modifier; Mg is used for LG-770 and Ba is used in LHG-8. For simplicity, we will refer to LG-770 glasses as KMAP for K-Mg-Al-P oxide glass and LHG-8 as KBAP for K-Ba-Al-P oxide glass. The properties and the preparation of these glasses are described elsewhere [5,6,13].

Two sets of samples were polished for this study. The first set of samples was the size of NIF amplifier slabs (77 x 44 x 4 cm) [5]. These samples were polished by Zygo Corporation using an aqueous slurry of 0.5 μm ceria (Hastilite PO^{TM}) on a pitch-bed circular polisher. Following polishing, each of the samples were sequentially removed from the pitch bed and immediately subjected to a different washing process to remove the polishing slurry from the sample. Variations in the cleaning efficiency of each of the washing processes resulted in a variation in the quantity of residual ceria remaining on the surface of each of the test specimens (see Table 1). Following storage at ~40% relative humidity for days to weeks, the samples were water rinsed, allowed to dry, and characterized with respect to surface quality (see section 2.2).

The post-storage (secondary) rinsing, of each of the full-size samples was performed by spraying each slab with approximately 5 liters of high purity water, which was delivered to the

surfaces of the slab at a rate of approximately 0.5 L/min. To allow the identity and quantity of glass corrosion products present, the rinsate from several separate full-sized samples were individually collected in a series of pre-cleaned and pre-weighed polypropylene buckets for later chemical analysis (see section 2.4).

The second set of samples was prepared by polishing a series of small (2.5 x 2.5 x 0.5 cm^3) glass coupons on an 8" Buehler polisher (ECOMET3 with an AUTOMET2 powerhead). Samples were prepared using four different slurries: (1) new (never used) Hastilite PO™ diluted 10:1 in water; (2) used slurry (same as used to polish the full-size samples); (3) new Hastilite PO™ diluted 10:1 in water adjusted to a pH of 10.5 using KOH; and (4) a new ZrO_2 (ZOX-PG Universal Photonics) slurry in water adjusted to a pH of 10.5 using NaOH. The slurry was recirculated using a peristaltic pump, throughout each of the polishing processes. The glass coupons were each polished for 9 hrs under a load of ~3.5 N on a rotating (50 rpm) pitch substrate. After polishing, a small amount of slurry was allowed to dry on the surface of the glass. The coupon samples were then stored at room temperature, in a 52% relative humidity environment. After one week, each coupon was thoroughly rinsed, using high purity water, and assessed for surface quality (see section 2.2).

2.2 Surface characterization

The topology of the glass surfaces of both the full-size and coupon samples was characterized visually, by atomic force microscopy (AFM), and by optical profilometry. AFM measurements were made in tapping mode using a Digital Instruments D5000 AFM equipped with an OTESP tip. Optical profilometry (μ-PMI) measurements were performed using a

WYCO NT2000 white light interferometer. Typically 5-9 locations, on each sample, were interrogated although only data from one representative location is typically presented.

2.3 Glass etch rate

The etch rate for both KMAP and KBAP glasses, as function of pH, was determined using a series of 2.5 x 2.5 x 0.5 cm^3 glass coupons. Each coupon was cleaned in an ultrasonic bath using an ethanol solvent and dried at 60^oC. After weighing, the glass coupons were soaked for a week at 23 °C in solutions that were buffered at pHs that ranged between 4.0 and 11.5. After re-cleaning & drying, the samples were reweighed and the material removal rate was determined.

2.4 Chemical analysis

The identity and quantity of the elemental constituents leached from the surface of the glass were determined by chemical analysis of the water used to rinse the slab (see section 2.1). This analysis was performed by evaporating each of the rinsate samples, in pre-cleaned Teflon beakers, to a suitable volume. Following concentration, each of the samples was acidified and the elements present were quantified using inductively coupled plasma-mass spectroscopy (ICP-MS) and by inductively coupled plasma-atomic emission spectroscopy (ICP-AES). The details of ICP-MS and the ICP-AES technology are described elsewhere [14].

The quantity of residual Ce remaining on the surface of several of the full-size samples was also estimated using chemical analysis techniques. This was done by painting a strippable polyurethane coating (Opticlean^{TM}) on the surface of several full-size samples after they had undergone initial washing and drying. After mechanical removal from the surface of the glass, portions of the coatings of known area were: 1) dry ashed in platinum crucibles, 2) chemically

dissolved in aqua-regia (a mixture of nitric and hydrochloric acid), and 3) diluted to a suitable volume. The quantity of Ce present in each sample was then quantitatively determined by ICP-MS.

3. Results

3.1 Observation of haze and the effect of slab washing

Table 1 summarizes the results for the full-size glass samples. After these slabs were polished, the slabs were immediately washed in a manner described in Table 1. Samples A and E were washed by wiping with a wet clean room cloth (Texwipe model 2412) after spraying with a small quantity (~15 ml) of deionized water and then wiped dry, much like one does for cleaning a window. Sample B was washed using the same method as Sample A except that immediately after drying the slab, it was re-rinsed with water. Sample C was washed by spraying with a copious amount of water (~10 L) but without wiping with a wet cloth. Sample D washed using copious amounts of water (~10 L) together with wiping with a wet cloth.

After initial washing and drying, the surface of each sample was visually inspected by illuminating the surface at a low angle using a high intensity fiber light in a dark room. All of the slabs, except for sample B, showed minimal light scattering. After storing each sample for days to weeks, the slabs were rewashed by spraying with DI water for 5 minutes. Upon reexamination, following the secondary rinse, the surfaces of several of the slabs showed a distinct increase in surface scatter. This observed scatter is referred to as surface haze, and was qualitatively described on a scale between 1 to 10, where 1 represents a haze-free surface and 10 represents haze equivalent of that observed on Sample A (see last column of Table 1). Notice that the haze level varied with both the initial cleaning method and the composition of the glass. For example, the KBAP glass was found to be much less susceptible to surface hazing than was

the KMAP glass. Of the KMAP samples, sample D, which had the most aggressive initial washing to remove residual slurry, had the least surface haze. Figure 1 compares photographs of the observed surface haze on samples A (haze level 10) and D (haze level 2). The areal density of residual slurry on the surface of samples A and D (see section 2.4) following initial washing were found to be $\approx 10^6$ CeO_{2-x} 0.5 μm particles/cm^2 for sample A and $\approx 10^3$ particles/cm^2 for sample D (Table 1).

3.2 Surface characterization

The surface topologies, as measured by μ-PMI and AFM, for several of the samples listed in Table 1 are shown in Fig. 2. The μ-PMI images are taken using an 834 x 834 μm^2 aperture, while the AFM images were taken over a 40 x 40 μm^2 aperture. The surfaces of the slabs exhibiting surface haze were found to contain very shallow (15-20 nm deep) surface pits, which range in diameter between 100 nm and 20 μm. The calculated root-mean-square (rms) roughness in the μ-PMI band (5 μm – 50 μm sized features) and the AFM band (100 nm – 1 μm sized features) are listed in Table 2.

AFM images of the small glass coupons, which were polished using a series of three different Hastilite PO^{TM} slurries, are shown in Fig. 3. The samples that were polished using a new (never used, pH=7) slurry did not show appreciable surface pitting (Fig. 3a). However, those samples polished with used slurry (pH=9.2) and a with a new slurry pH adjusted, with KOH, to a pH of 10.5 resulted in surfaces which had pitting similar to that observed in the full-size glass samples (Fig. 3b-c). Surface pitting was also observed using a completely different slurry system at high pH; Fig. 4 shows a μ-PMI image of the glass coupon polished with a ZrO_2 (which was pH adjusted to 10.5 using NaOH) slurry.

3.3 Chemical analysis and glass etch rate

The chemical analysis of the secondary rinsate (see sections 2.1 and 2.4) from full-sized samples A, D and E are summarized in Table 3. Each component in the Table is listed on the basis of the quantity of equivalent oxide removed, the percentage of each component removed, and percentage of each component removed relative to the composition of each glass. Notice that sample A, which was the most highly pitted and hazed sample, had the greatest total quantity of material removed during the secondary rinse.

The etch rate (in nm/hr) for the two glass types, as a function of pH, is shown in Fig. 5. The etch rate for both glass types increases strongly with increasing pH. However, KMAP glass etches faster than the KBAP glass at any given pH.

4. Discussion

4.1 Scatter and pit density

As discussed above, both the visible haze and the density of pits appear to correlate with elevated levels of residual ceria. This suggests that residual ceria may be responsible for pitting the surface of the phosphate glass and that the pits are responsible for light scattering, or haze. The relationship between the pitting of the surface and light scatter are considered in this section, while the distribution of pit sizes and the mechanism of pit formation are considered in latter sections.

It is well known that light can be scattered by a surface if the sizes of the imperfections are comparable in size to the wavelength of light (λ). Quantitatively, the surface scatter (S) scales with the average surface roughness (δ_T) [15] as:

$$S = \left(\frac{4\pi \delta_T}{\lambda} \right)^2 . \quad (1)$$

In the case where features of differing size must be considered, the surface roughness can be taken as the root mean square (rms) roughness:

$$\delta = \sqrt{\frac{1}{N} \sum_{i=1}^{N} z_i^{\,2}} \quad (2)$$

where N are discrete, equally-spaced measured points (the minimum spatial wavelength) along a surface, and z is the local surface height above or below the mean height of the surface. Note that the computed of the rms roughness will depend on total length of the surface profile (the maximum spatial wavelength), the surface area being averaged over (lateral resolution), and distance between data points (minimum spatial wavelength) [15].

In the present analysis, surface roughness measurements can be computed from topology measurements made by both AFM and μ-PMI. However, the feature scale over which each of these techniques is sensitive is quite different. For the present work, the band of features observed in the AFM data typically run between 100 nm and 1 μm, while the features present in the μ-PMI range are between 5 μm and 50 μm. The overall surface roughness, δ_T, can be estimated by adding the rms roughness over the two spatial bands (δ_1 from the AFM measurements and δ_2 from the μ-PMI measurement) in quadrature:

$$\delta_T = \sqrt{\delta_1^{\,2} + \delta_2^{\,2}} . \quad (2)$$

However, scatter is typically determined for spatial wavelengths down to ~λ [15]. For visible light (λ ~ 550 nm) and for the NIF laser light (λ = 1053 nm), the AFM band (100 nm to 1 μm) measures features that are below λ and it is not valid to use Eq. 1-3. Hence, the scatter only due to μ-PMI band (5 μm – 50 μm) is calculated in Table 2. As shown in Table 2, the calculated

scatter (S) scales with the observed haze, suggesting the pits are the major source of the observed scatter.

4.2 Distribution of Pit Sizes

Image analysis of the surface topology (shown in Fig. 2), of several of the large glass samples, was performed to determine the areal density of pits as a function of pit diameter (see Fig. 6). Although the distribution of pit diameters is quite wide, ranging from 100 nm to 20 μm, the depth of the pits is essentially constant (typically 15-20 nm). As shown in Fig. 6, there is a plateau in the distribution in the 100-300 nm size range. This suggests that the fundamental pit size is in the range of 100-300 nm. This fundamental pit size (~100 nm x 15 nm deep) has a shape and size that is similar to the geometrical contact area of a spherical 0.5 μm diameter particle penetrating 15 nm into the glass surface. This suggests that the pits are likely formed at the contact boundary between slurry particles and the glass surface.

The pit distribution (Fig. 6) outside the plateau region can be described by a simple power law expression of the form:

$$n(d) = A d^{m} \tag{4}$$

where n is the areal pit density (#/cm^2) within a specific size range of pits diameters (d), m is the power law dependence of that distribution, and A is a fitting constant. The AFM and μ-PMI data both can be fit the same power law exponent, suggesting that the pit distribution is unimodal and suggesting a single mechanism is responsible for their formation. A likely explanation for the broad range of pit sizes is that the larger pit sizes result from the clustering of smaller pits. This is apparent by comparing Fig. 7, which shows an optical micrograph of some CeO_{2-x} particles sitting on the surface of the laser glass, with the larger pit observed in the top of Fig. 2b.

4.3 The Mechanism of pit formation

The presence of surface pitting implies the presence of a localized physical or chemical process at the surface of the glass. Using elastic Hertzian mechanics to equate the load energy (from the indenting particle) with the elastic strain energy (in the glass), the load (P) required to form the fundamental pit size by physical means is given by [16]:

$$P = \frac{3}{4}\frac{a^3 E_s}{k\,r} \tag{5}$$

where k is a material constant ~1, E_s is the elastic modulus of the phosphate glass (50 GPa), *a* is the contact area (or fundamental pit diameter) (~150 nm), and r is the radius of the contacting particle (250 nm). The determined value of P is $5\text{x}10^{-4}$ N. This load is orders of magnitude higher than the load caused by: (1) the weight of the particle (10^{-15} N); (2) the capillary pressure from water evaporation at the glass-particle interface (10^{-8} N); and even (3) the effective weight of the glass on a single particle during polishing (10^{-7} N). Hence mechanical loads alone cannot be responsible for the formation of the pits. That is a chemical mechanism must be primarily responsible.

The removal of silica glass by CeO_{2-x} particles has been examined in the CMP literature [7-12]. The key features of this mechanism involve stress-enhanced water diffusion into the glass [10], mobile alkali metal cations diffusing out of the glass [7], and the development of a fractured and chemically modified surface layer. The rate of glass removal (R in thickness/time) during polishing is defined by Preston's equation [17]:

$$R = K\,\sigma\,v \tag{6}$$

where σ is the applied pressure, v is the linear velocity of the polishing pad with respect to the optic (cm/sec), and K is the Preston coefficient. For ceria polishing fused silica, the Preston coefficient is 2 x 10^{-14} cm^2/dyne (2 x 10^{-9} cm^2/N) [17]. Using typical loads and linear velocities, Cook showed each individual ceria particle removes only 1/24 of a molecule (SiO_2 unit equivalent) of glass per impact [7]. Phosphate glass, which has a Preston coefficient of ~4 x 10^{-14} cm^2/dyne (4 x 10^{-9} cm^2/N), would have a similar removal rate. Hence dried stagnant slurry causing pits leads to much greater material removal, compared with a moving, higher mechanically loaded passing across the glass surface.

Given mass transport considerations, it is unlikely that the pit formation is due to a solid-state reaction. It is more likely that there is condensed liquid present, at the particle-glass interface, which both mediates mass transport and can lead to local hydrolysis of the phosphate chains making up the glass. The presence of such a condensed phase, in small pores or capillaries, is predicted by the Kelvin equation [18]:

$$\frac{P_w}{P_o} = \exp\left(\frac{-2\gamma V_l \cos\phi}{r_m RT}\right) \tag{7}$$

where P_w is the water vapor pressure (Pa), P_o is the saturation vapor pressure (Pa) at temperature (T), γ is the water surface energy (72 x 10^{-3} N/m), ϕ is the contact angle, and V_l is molar volume of water (18 cm^3/mole). This equilibrium relationship predicts that at some water vapor pressure, well below saturation (i.e., relative humidity below 100%), a pocket of liquid exists in the pores of the ceria particles and as well as at the interface between the glass and the particle. Thus the presence of the residual ceria provides a means of localizing a condensed aqueous phase, on the surface of the glass.

The effect that the residual slurry has on the quantity of glass removed from the surface of several full-sized test samples is shown in Table 3 and Fig. 8. The effective thickness of glass removed from each sample (Fig. 8) was calculated based on the total quantity of phosphorous that was recovered during the secondary rinse of each of the slabs (see Table 3), together with the physical dimensions and density of each glass sample. As shown in Fig. 8, the quantity of material removed depends strongly both on the quantity of residual slurry remaining on the slab following initial (post polishing) washing (see Table 3) and the composition of the glass (KMAP versus KBAP). For example Sample A, which had a high pit density, had 100x more material removed compared to Sample D, which had a low pit density and comparatively low quantity of residual Ce. Clearly, the amount of glass degradation scales with the residual slurry or ceria particle / glass surface contact area.

Additional data from Table 3 is also shown in Fig. 9, in which the relative amount of each of the glass components (on an oxide basis) recovered from the secondary rinse with respect to the nominal glass composition is shown. If the bar is to the right of the origin, then the indicated component was present, in the rinsate, in excess compared to the nominal glass composition. K was preferentially leached from both the KMAP and KBAP glasses. This is consistent with previous studies of compositional differences in the bulk and surface composition of phosphate glasses [22]. It is also interesting to note that the Group II modifier appears to have been much more retained in the case of the KBAP glass compared to the KMAP glass (see section 4.4).

As described earlier, the results of the small-coupon polishing tests indicate that the pH of the slurry appears to be a key parameter with respect to the formation of surface pits. The used slurry (pH≈9.2) and the KOH adjusted slurry (pH≈10.5) led to pitting, while a new slurry (pH≈7) did not. Surface pitting was also observed using a completely different slurry system at high pH;

Fig. 4 shows a μ-PMI image of the coupon polished with a ZrO_2 (which was pH adjusted using NaOH to 10.5) slurry. These results appear to be consistent with the observation that dissolution rates of these glasses increase dramatically with pH (Fig. 5).

The details of chemical reaction that takes place at the particle-glass interface that results in pitting are not fully understood. None-the-less the present results appear to be largely consistent with previous results concerning the bulk dissolution of phosphate glasses. Bunker [19] has shown the dissolution of meta-phosphate glasses occur as the result of the hydrolysis of the polymeric chains of the glassy network. Previous studies of the interaction of water with phosphate glass suggest that water first hydrolyzes bonds between the non-bridging oxygens and various metallic modifiers. Hydrolysis continues with the scission of P-O-P bonds that make up the backbone of the metaphosphate glass structure, decreasing the length of the phosphate chains [19,20]. Based on results obtained by liquid chromatography [21], it has been shown that phosphate chains less than 20-30 units are readily soluble in water. Such a hydrolysis mechanism is consistent with the observation that pits are only exposed upon (secondary) washing with water after letting the slurry dry on the surface. Note rinsing with ethanol or acetone did not expose the pits. Schematic summarizing the proposed sequence and mechanism for pit formation is illustrated in Fig. 10.

4.4 The relative durability of KMAP vs KBAP glass

The two glasses examined in this study, KMAP and KBAP exhibit significant differences in their propensity to pit and thus haze. The most important compositional difference between the two glasses is the Group II modifier used in each glass; the KMAP glass uses Mg as the Group II modifier, while the KBAP glass uses Ba. From the point of view of laser performance,

the KMAP glass exhibits a higher emission cross-section and thus has a somewhat higher gain than does the KBAP glass [5]. The KBAP, however, provides better performance characteristics with respect to a number of mechanical and chemical durability criteria such as resistance to weathering and glass corrosion [23,24,25]. As discussed above, the KMAP glass has a higher etch rate at given pH than does the KBAP glass. Similarly the KMAP glass tends to polish (i.e., have a larger Preston Coefficient) more quickly than does the KBAP glass.

The two glasses, used in this study, are highly engineered, multi-component materials that have differences in composition other than the Group II modifier. However, there are important differences in the chemistry of Mg and Ba that may be responsible for the differences in the various measures of chemical durability, including pitting, which are observed in these two glasses. Dissolution of phosphate glasses is thought to involve initial hydrolysis of bonds connecting metallic modifiers and oxygen atoms associated with the phosphate chains making up the glass. The specific strength of the bond between the Group II modifiers and oxygen in these glasses is not known. However, standard tabulations of bond strengths, such as those given by Kerr and Trotman-Dickenson [26], suggest that the Ba-O bond is stronger than is the Mg-O bond. Similarly, the ionic radius, as estimated by Pauling [27], of Ba^{2+} is over twice that of the Mg^{2+} ion (1.35 versus 0.65 Å). As a result of its smaller size, the Mg^{2+} ion is much easier to hydrate than is the Ba^{2+} ion. This is reflected in the relative values of the enthalpies of hydration of the Mg^{2+} (1960 KJ/mol) ion compared to the Ba^{2+} (1340 KJ/mol) ion [28]. This trend is evident in the chemical analysis of the rinsate shown in Fig. 9. Note, in Figure 8 that the Mg (from the KMAP glass) was preferentially leached into the rinse solution relative to the nominal glass composition, while the fraction of Ba in the rinse solution (from the KBAP glass) was deficient relative to the nominal glass composition.

5. Conclusions

The observed haze (i.e., surface scatter) on Nd-doped metaphosphate glasses is a result of shallow (15 nm) pits, ranging in size between 100 nm to 20 μm in diameter, that are formed on the surface of the glass. The number density, shape and size distribution of the pits correlate with residual slurry particles that can remain on the surface of the glass following polishing. The mechanism of pit formation involves the reaction of the glass surface with a condensed aqueous phase that is trapped at the glass-slurry particle interface owing to capillary condensation. In the presence of a condensed aqueous phase, glass modifiers such as K^{1+} and Mg^{2+} leach from surface of the glass and hydrolysis of the phosphate chains likely occurs. As a result, local regions are formed on the surface of the glass which are much more water-soluble than the native glass matrix. Upon subsequent contact with water, these areas are preferentially exposed as pits (Fig. 11). The composition of the condensed phase, specifically pH as well as the nature of the glass modifiers, play important roles in controlling the extent of the reaction. Ensuring the glass surfaces are thoroughly washed immediately after polishing, and not allowing the slurry to 'dry' on the surface, is an effective means of preventing localized pit formation, and thus the haze from forming on the glass surface.

ACKNOWLEDGEMENTS

This work was performed under the auspices of the U.S. Department of Energy by University of California, Lawrence Livermore National Laboratory under Contract W-7405-Eng-48. The authors would like to thank L. Summers (AFM), W. House (μ-PMI), C. Carroll (μ-PMI), F. Zaka

(ICP-MS and ICP-AES analysis), and E. Lindsey (SEM). The authors would also like to thank J. Campbell, C. Thorsness, M. Riley, G. Rogowski, C. Weinzapfel, S. Frieders, D. Dodson, R. Cabecerious, and L. Auyang for useful discussions and experimental assistance.

References

[1] J. Murry, "Overview of the National Ignition Facility", SPIE 3492 Supplement (1998) 1.

[2] C. Stolz, J. Menapace, M. Borden, A. Slomba, C. Kikka, S. Gelman, "Status of Optical Finishing for the National Ignition Facility", in Optical Fabrication and Testing, OSA Technical Digest (2002) 67.

[3] E. Moses, J. Campbell, C. Stolz, C. Wuest, "The National Ignition Facility: The World's Largest Optics and Laser System", SPIE 5001 (2003) 1.

[4] H. Karow, Fabrication Methods for Precision Optics, John Wiley & Sons, Inc., New York (1993).

[5] J. H. Campbell, T. I. Suratwala, "Nd-doped phosphate glasses for high-energy/high peak power lasers", J. of Non-Cryst. Solids, 263&264 (2000) 318.

[6] J. H. Campbell, T. I. Suratwala, C. B. Thorsness, J. S. Hayden, A. J. Thorne, J. M. Cimino, A. J. Marker III, K. Takeuchi, M. Smolley, G. F. Ficini-Dorn, "Continuous melting of phosphate laser glasses", J. of Non-Cryst. Solids, 263&264 (2000) 342.

[7] L. Cook, "Chemical Processes in Glass Polishing", J. Non-Cryst. Solids 120 (1990) 152.

[8] T. Izumitani, in: Treatise on Material Science and Technology, Vol 17, eds. M. Tomozawa and R. Doremus, Academic Press, New York (1979) 115.

[9] L. Holland, The Properties of Glass Surfaces, Chapman and Hall, London (1964).

[10] M. Tomozawa, K. Yang, H. Li, S. Murarka, “Basic Science in Silica Glass Polishing”, Mat. Res. Soc. Symp. Proc. 337 (1994) 89.

[11] M. Tomozawa, “Oxide CMP mechanisms”, Solid State Technology (July 1997) 169.

[12] N. Brown, “Some Speculations on the mechanism of abrasive grinding and polishing”, Mat. Res. Soc. Symp. Proc. 337 (1994).

[13] T. Suratwala, C. Thorsness, J. Campbell, S. Krenitsky, J. Cimino, A. Thorne, J. Hayden, K. Takeuchi, K. Suzuki, K. Yamamoto, “Technical advances in the continuous melting of phosphate laser glass,” in Inertial Fusion Sciences and Applications, ed. K. Tanaka, D. Meyerhofer, J. Meyert-ter-Vehn, Elsevier (2002) 540.

[14] D. Skoog, J. Leary, Principles of Instrumental Analysis, 4th Edition, Saunders College Publishing (1992).

[15] J. Bennett, L. Mattson, Introduction to Surface Roughness and Scattering, Optical Society of America, Washington, D.C. (1989).

[16] B. Lawn, “Fracture of Brittle Solids- 2nd Edition”, Cambridge University Press, Cambridge,UK (1993).

[17] F. Preston, “Theory and Design of Plate Glass Polishing Machines”, J. Soc. Glass Technol. 11 (1927) 124.

[18] P. Atkins, Physical Chemistry, 5th Ed, Oxford University Press (1994).

[19] B. Bunker, G. Arnold, J. Wilder, “Phosphate Glass Dissolution in aqueous solutions”, J. Non-Cryst. Solids 64 (1984) 291.

[20] J. S. Hayden, A.J. Marker III, T. I. Suratwala, J. H. Campbell, "Surface tensile layer generation during thermal annealing of phosphate glass," J. of Non-Cryst. Solids, 263&264 (2000) 228.

[21] R.K. Brow, “Review: the structure of simple phosphate glasses”, J. Non-Cryst. Solids 263 & 264 (2000) 1.

[22] W. Meisel, D. Sprenger, P. Gutlich, “Surface versus bulk composition of a phosphate glass”, Surface and Interface Science 22 (1994) 267.

[23] Crichton, M. Tomozawa, J. Hayden, T. Suratwala, J. Campbell, "Sub-Critical Crack Growth in a Phosphate Laser Glass," J. Amer. Cer. Soc. 82(11) (1999) 3097.

[24] T. I. Suratwala, R.A. Steele, G.D. Wilke, J.H. Campbell, "Effects of OH content, water vapor pressure, and temperature on sub-critical crack growth in phosphate glass", J. of Non-Cryst. Solids, 263&264 (2000) 213.

[25] P. Ehrmann, and J. H. Campbell, Chemical Weathering of Phosphate Glasses, LLNL Report, UCRL-PRES-155863 (2004).

[26] J.A. Kerr and A.F. Trotman-Dickenson “Strengths of Chemical Bonds” in “Handbook of Chemistry and Physics” 57th Edition, CRC Press 1976.

[27] L. Pauling, “The Nature of the Chemical Bond”, 3rd Edition, Cornell University Press, 1960.

[28] R.B Heslop and K. Jones “Inorganic Chemistry – A Guide to Advanced Study”, Elsevier Scientific Publishing 1976.

Table 1: Description and results of the phosphate glass samples after final polishing and secondary rinsing.

Glass Type	Glass Sample	Cleaning procedure after polishing	Water Sheeting on surface	Residual CeO_{2-x} particles on surface (#/cm^2)	μ-roughness (δ_2) (nm)	Level of Haze*
KMAP	A	Short water rinse (15 ml)	---	10^6	1.04	10
	B	Water rinse (~10 L)	---	---	0.65	9
	C	Surface always wet + water rinse (~10 L)	Moderate	---	0.25	3
	D	Surface always wet + wet cloth scrub + water rinse (~10 L)	Good	10^3	0.20-0.25	1-2
KBAP	E	Short water rinse (15 ml)	---	---	0.27	2

* 1 = no Haze; 10 = Haze similar to Sample A

Table 2: Calculated pit area, rms roughness, and scatter using surface topology data shown in Fig. 2.

Glass	From AFM images		From μ-PMI images			Haze scale (qualitative)
	Pit area	Roughness (δ_1) (rms) (nm)	Pit area	Roughness (δ_2) (rms) (nm)	Calculated Scatter Fraction (Eq. 1)	
Sample A	6.7 %	4.55	2.1 %	1.04	**5.6×10^{-4}**	**10**
Sample B	8.1 %	2.75	0.6 %	0.65	**2.2×10^{-4}**	**6**
Sample D	0.4 %	*	0 %	0.23	**0.3×10^{-4}**	**1**

*not calculated/ vibration in image dominating

Table 3: Summary of measured chemical products from slab rinsing tests.

Glass	Glass Sample	Oxide	µg/slab removed (oxide basis)	Removed material Oxide (wt %)	Base glass Oxide (wt %)	% relative to base glass
KMAP	A	P_2O_5	22300	59.7	70.8	-16%
		K_2O	7526	23.3	15.4	51%
		Al_2O_3	448	10.1	6.7	51%
		Nd_2O_3	160	4.7	4.7	0%
		MgO	1075	2.2	2.4	-8%
		BaO	3.3	na	na	na
		Ce_2O_3	6.3	na	na	na
KMAP	D	P_2O_5	89	70.8	70.8	0%
		K_2O	35	23.9	15.4	55%
		Al_2O_3	15	1.4	6.7	-79%
		Nd_2O_3	7	0.5	4.7	-89%
		MgO	3	3.4	2.4	42%
		BaO	0	na	na	na
		Ce_2O_3	1.2	na	na	na
KBAP	E	P_2O_5	759	74.8	63.6	18%
		BaO	11.9	1.2	13.4	-91%
		K_2O	183	18.0	11.1	62%
		Al_2O_3	46.6	4.6	7.7	-40%
		Nd_2O_3	13.9	1.4	4.2	-67%
		MgO	19.8	na	na	na
		Ce_2O_3	2.7	na	na	na

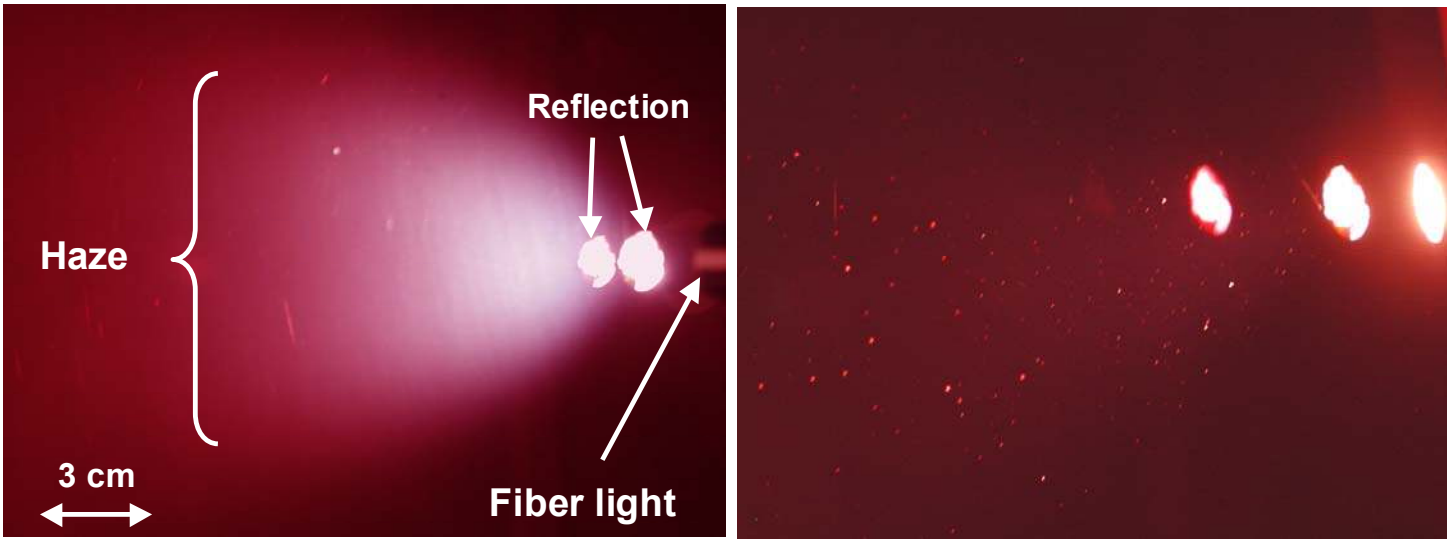

Figure 1: Photographs of the surface scatter observed from (a) a highly hazed phosphate glass sample (Sample A) and (b) an essentially haze-free sample (Sample D). Images were taken in a dark room upon viewing the diffuse reflectance from a high intensity fiber light. The particles observed in (b) were intentionally left on surface in order to distinguish (i.e, focus on) the surface.

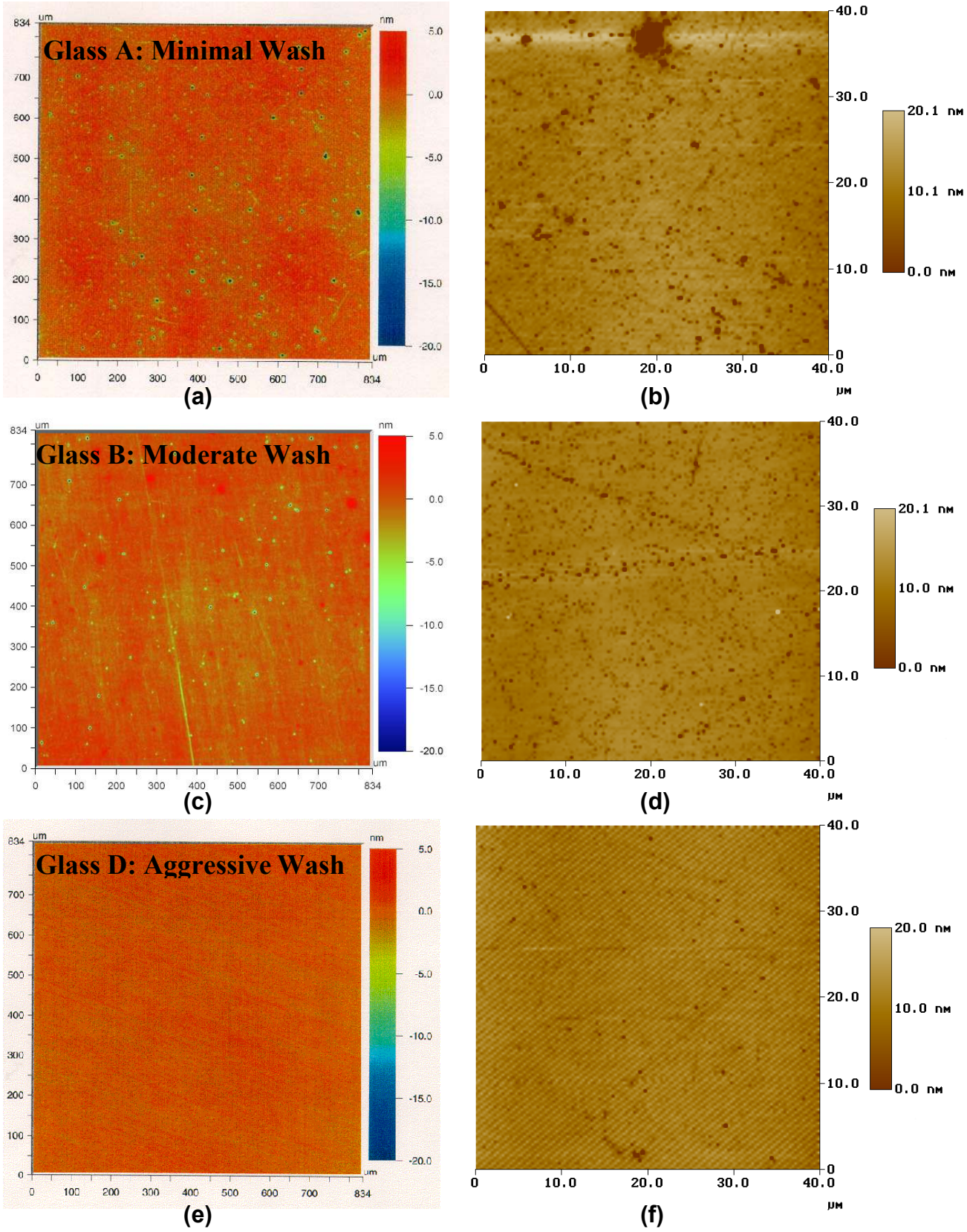

Figure 2: μ-PMI (left side) and AFM (right side) images for three of the full-sized KMAP glass samples: (a-b) Sample A, (c-d) Sample B, and (d-e) Sample D.

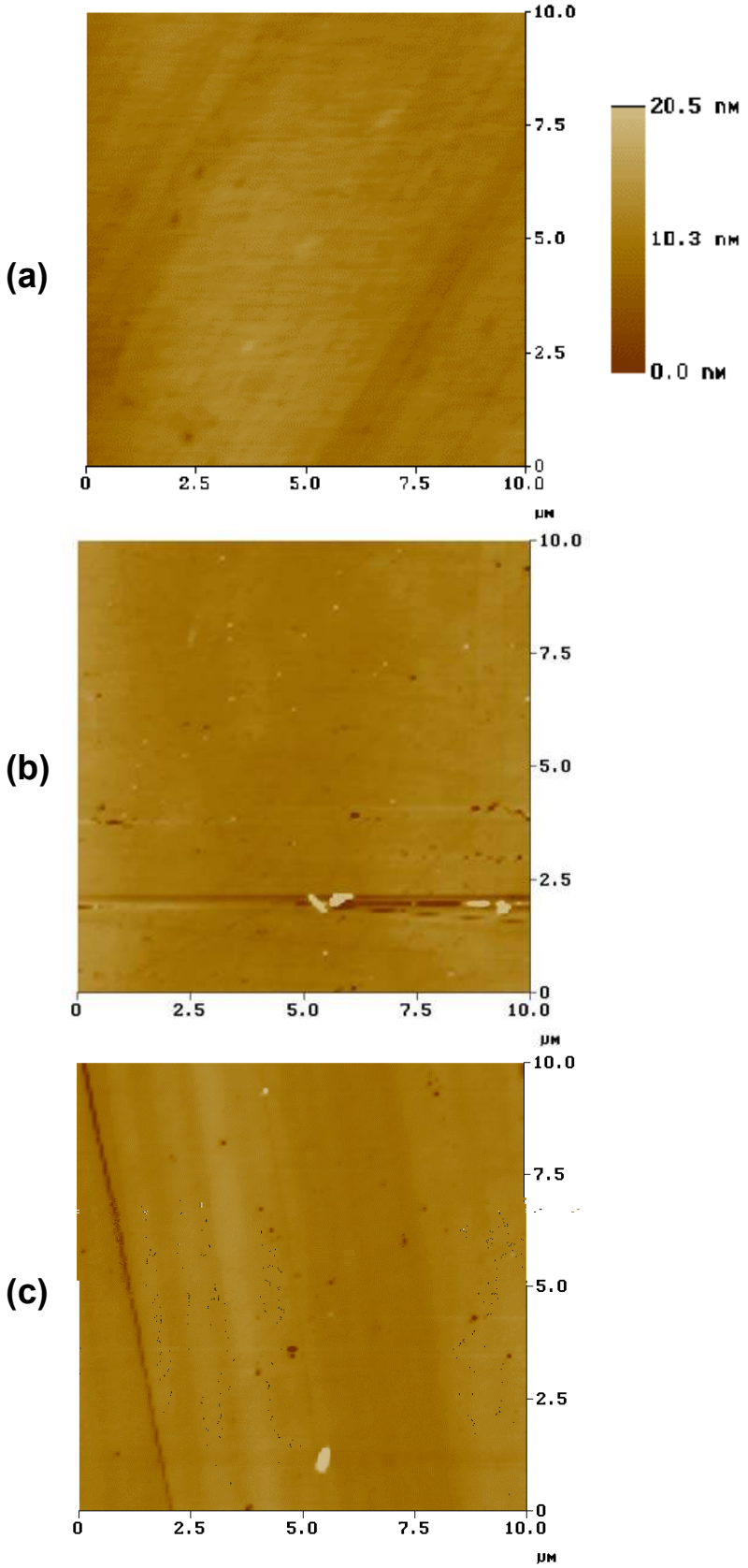

Figure 3: AFM images of KMAP glass coupons polished with (a) new, (b) used, and (c) new + KOH Hastilite PO^{TM} slurry and then washed after allowing dried residual slurry to remain on the surface for 1 week.

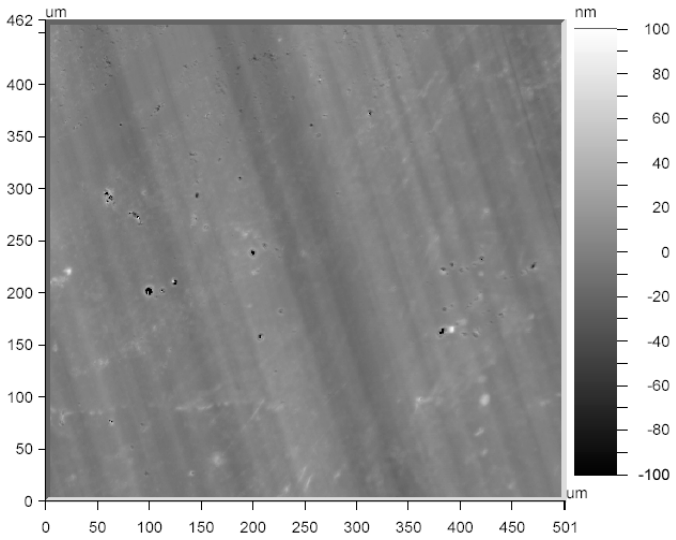

Figure 4. μ-PMI image of a KMAP glass coupon that was polished with new ZrO_2 slurry + NaOH and then washed after allowing dried residual slurry to remain on the surface for 1 week.

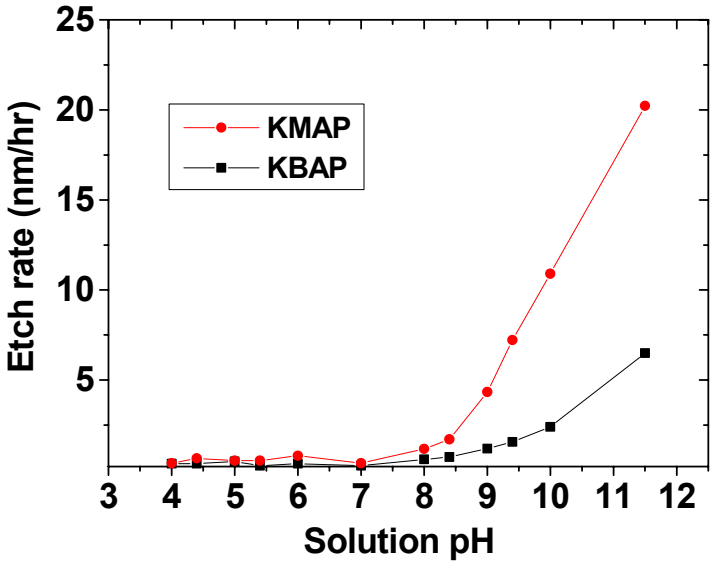

Figure 5. Etch rate as a function of pH for KMAP and KBAP glasses.

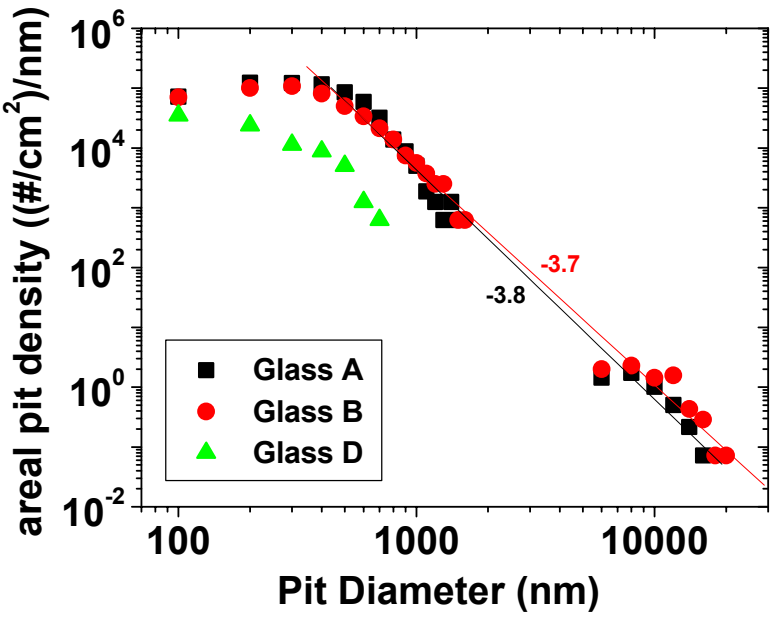

Figure 6: Pit size distribution for Samples A, B and D determined from images shown in Fig. 1. The lines are power law fits to the data outside the plateau region using Eq. 4.

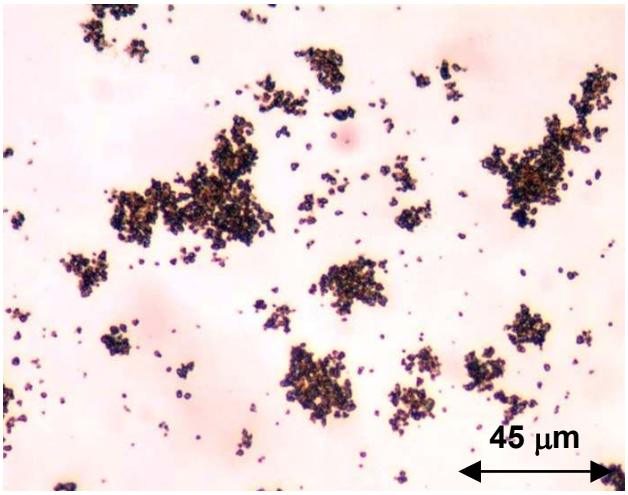

Figure 7: Optical micrograph of Hastilite PO^{TM} CeO_{2-x} particles sitting on surface of KMAP. Notice the clustering that takes place and compare with large pit at the top of Fig. 3b.

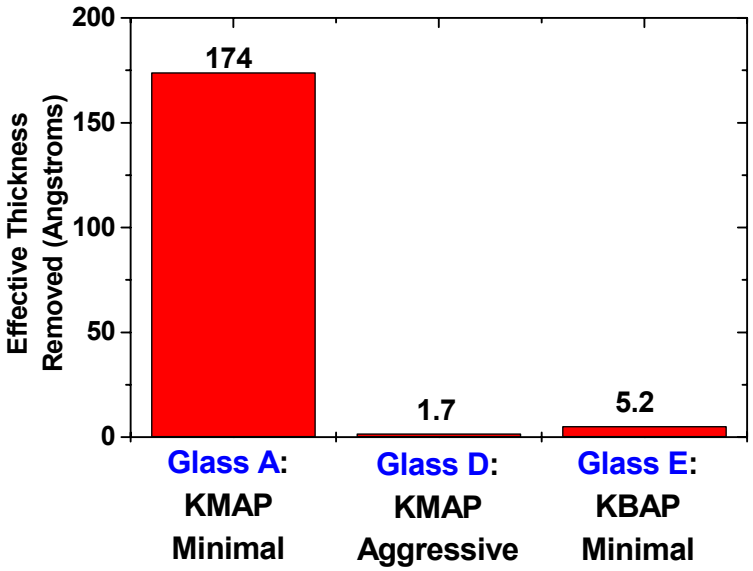

Figure 8: Comparison of effective glass thickness removed (calculated data in Table 2) upon washing amplifier slab with water.

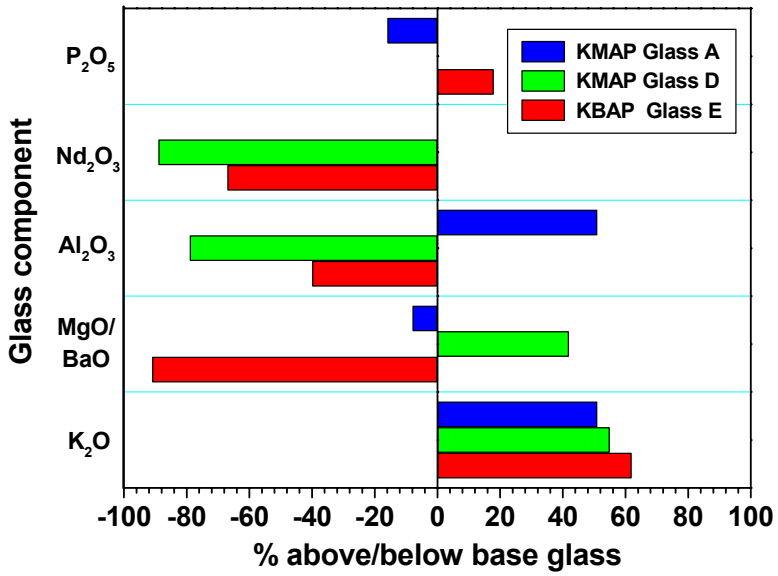

Figure 9: Relative amount of each glass component (with respect to the bulk glass) that was removed during secondary rinsing of Samples A, D & E (using data from Table 2).

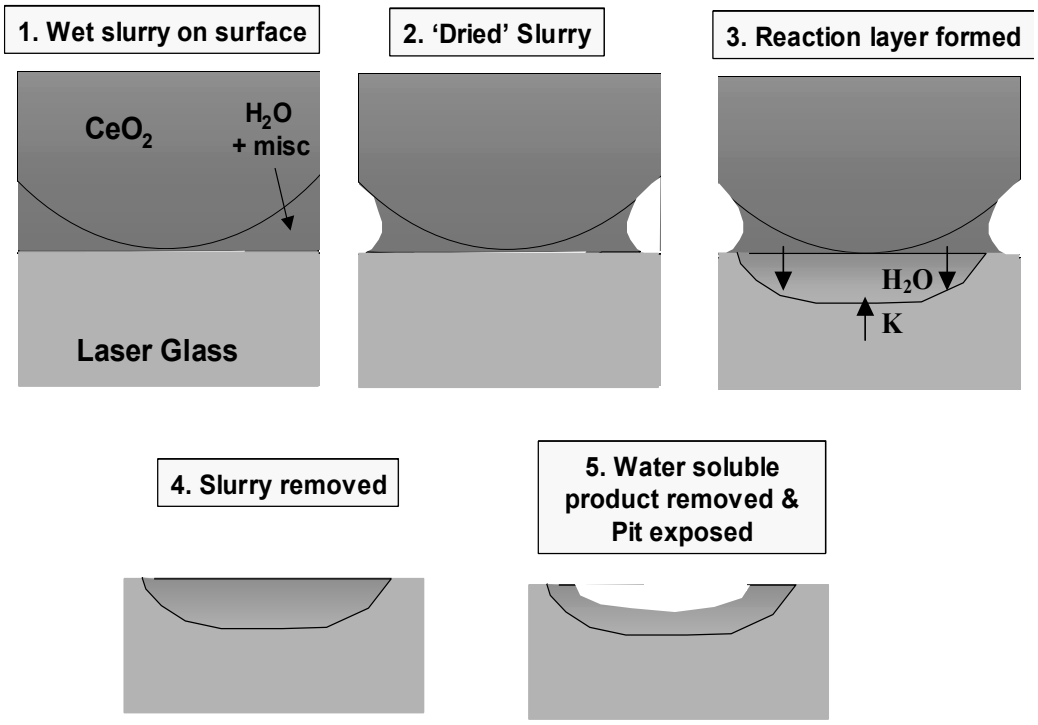

Figure 10: Schematic illustration of pit formation in phosphate glass when residual slurry is 'dried' on surface.

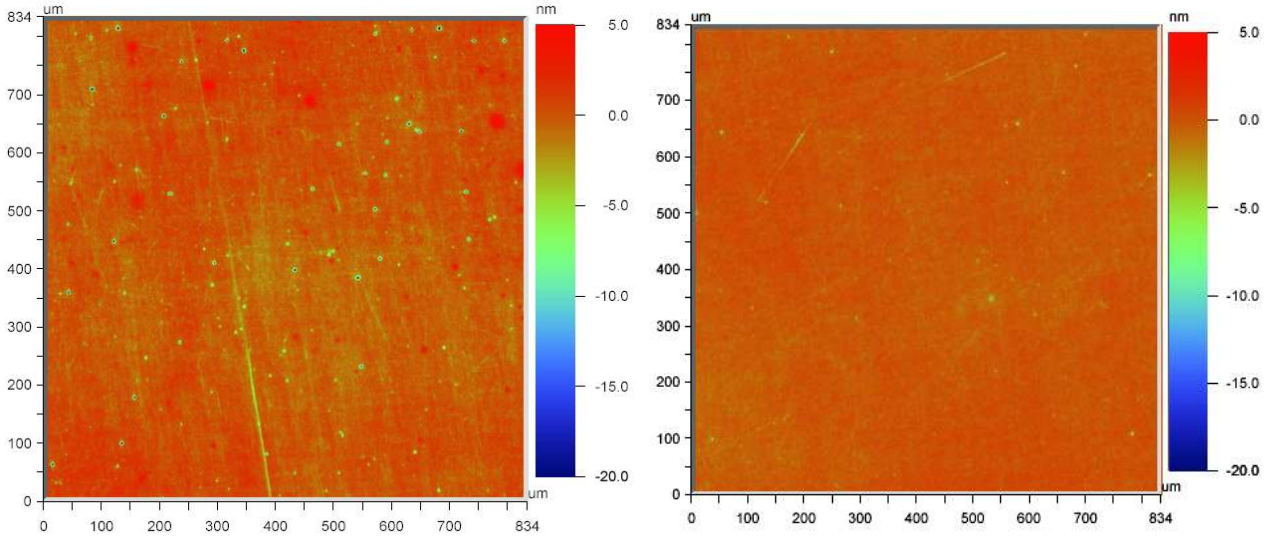

Figure 11. μ-PMI images comparing the degree of pitting observed for Sample A [KMAP (δ_2=0.65 nm)] and Sample E [KBAP (δ_2=0.27 nm)].